Neuroradiology (2008) 50:411–421
DOI 10.1007/s00234-007-0350-x

INTERVENTIONAL NEURORADIOLOGY

Impact of aneurysmal geometry on intraaneurysmal flow: a computerized flow simulation study

Istvan Szikora · Gyorgy Paal · Adam Ugron · Ferenc Nasztanovics · Miklos Marosfoi · Zsolt Berentei · Zsolt Kulcsar · Wickly Lee · Imre Bojtar · Istvan Nyary

Received: 19 July 2007 / Accepted: 28 November 2007 / Published online: 5 January 2008

Abstract
Introduction This study was performed to assess the effect of aneurysm geometry on parameters that may have an impact on the natural history of intracranial aneurysms, such as intraaneurysmal flow pressure and shear stress.
Methods Flow was simulated in 21 randomly selected aneurysms using finite volume modeling. Ten aneurysms were classified as side-wall aneurysms, with either single-sided or circumferential involvement of the parent artery wall, and 11 as bifurcation aneurysms (symmetric or asymmetric), with an axis either perpendicular or parallel to the parent artery. The flow patterns were classified as either jet or vortex types (with regular or irregular vortex flow). Pressures and shear stresses were characterized as evenly or unevenly distributed over the aneurysm wall and neck.
Results All side-wall and four of the bifurcation aneurysms with a perpendicular axis had a vortex type flow pattern and seven bifurcation aneurysms with a parallel axis (four symmetric and two asymmetric) had a jet flow pattern. Jet type flow was associated with an uneven pressure distribution in seven out of seven aneurysms. Vortex type flow resulted in an even pressure distribution in five out of six aneurysms with an irregular flow pattern and six out of eight with a regular flow pattern. No firm relationship could be established between any geometrical type and shear stress distribution. Only 1 of 14 aneurysms with a perpendicular axis, but 4 of 7 aneurysms with a parallel axis, had ruptured.
Conclusion Aneurysm geometry does have an impact on flow conditions. Aneurysms with a main axis parallel to the parent artery have a tendency to have a jet flow pattern and uneven distribution of unsteady pressure. These aneurysms may have a higher rate of rupture as than those with a main axis perpendicular to the parent artery.

Keywords Aneurysm geometry · Computational fluid dynamics · Flow simulation · Aneurysm natural history

I. Szikora · M. Marosfoi · Z. Berentei · Z. Kulcsar · W. Lee · I. Nyary
National Institute of Neurosurgery,
Budapest, Hungary

G. Paal · A. Ugron · F. Nasztanovics · I. Bojtar
University of Technology and Economics,
Budapest, Hungary

I. Szikora (✉)
Interventional Neuroradiology, National Institute of Neurosurgery,
Amerikai ut 57,
Budapest 1145, Hungary
e-mail: h13424szi@ella.hu

Introduction

The indication for invasive treatment of unruptured aneurysms represents a clinical challenge because of the limited knowledge of the natural history and the relatively high risk of preventive procedures such as open surgery or endovascular treatment. In current clinical practice, decisions are generally based on history, aneurysm location and size. Recent clinical studies have demonstrated a relationship between the risk of rupture and history, aneurysm size and location. These results suggest that aneurysms in patients with a history of previous subarachnoid hemorrhage (SAH) and those larger than 7 mm in diameter located in the anterior circulation or located in the posterior circulation have a higher risk of rupture [1, 2].

While the correlation between size and rupture risk might be substantiated by fluid dynamics (Laplace's law), the significance of aneurysm location and patient history

remains unexplained. It seems likely, that other factors, such as intra- and extraaneurysmal flow conditions may play a role in aneurysm growth and the likelihood of rupture. Intraaneurysmal flow patterns have been extensively studied using angiography [3], transparent aneurysm models [4–8] and lately computational fluid dynamics (CFD) [9–14]. Material differences within the perianeurysmal microenvironment have been suggested as explaining the significance of location [15–17]. Aneurysm geometry might be one of the key factors responsible for intraaneurysmal flow that in turn may play a role in aneurysm growth and rupture. Hence location may indirectly influence rupture risk by affecting geometry through the perianeurysmal environment. Multiple aspects of aneurysm geometry, such as side wall or bifurcation type, relationship to side branches and parent vessel curvatures [18], and the aspect ratio [7, 19] have been studied. We have previously demonstrated that other geometrical factors, such as the diameter and height of the neck, significantly influence the flow pattern in computer aneurysm models [20].

We report here our analysis of the effects of multiple geometrical parameters, including the type of aneurysm, the angle between the aneurysm and parent vessel and aneurysm symmetry in relation to side branches, on flow patterns in real human intracranial aneurysms using finite volume modeling and computational flow simulation.

Methods and materials

A total of 21 aneurysms were retrospectively selected making sure that different morphological types (such as side wall or bifurcation aneurysms) were equally represented in the entire group. During the selection process, the clinical history of the patients and anatomical locations of the aneurysms were not taken into consideration. In order to achieve good flow visualization, very small aneurysms (<6 mm) were not included in this study.

Conventional 2-D and 3-D rotational angiography studies were obtained in all aneurysms using a GE LCV+ digital subtraction angiography unit and an Advantage Windows workstation with ADW 4.2 reconstruction software. The aneurysm with a relevant length of both the proximal and distal parent artery was selected by the interventional neuroradiologist members of the team. The 3-D image database was then converted to a geometrical database from which a tetrahedral mesh was produced using in-house software. Flow was then simulated on the resulting finite volume model assuming the circulating fluid as Newtonian and incompressible with a specific density of 1,050 kg/m^3 and viscosity of 0.003 kg/m s. Vessels and aneurysms were considered as rigid tubes. Flow was simulated using the ANSYS CFX 10 commercial software that uses a high resolution scheme providing second-order spatial accuracy which drops to first-order near discontinuities. Time discretization was provided by a backward Euler scheme resulting in second-order accuracy. The solver uses a coupled, transient numerical scheme, and colocated grid arrangement. Convergence acceleration was obtained using the additive correction algebraic multigrid method. Grid independence was established by producing similar but artificial geometries where the mesh density could be controlled easily. By thorough mesh studies performed on the artificial geometries a typical error of less than 5% was found with a maximum of 10% in the worst places. Models comprised an average of 300,000 elements.

The analytic cardiac cycle was 0.8 s with a time step of 0.02 s so that one cycle comprised 40 time steps. A total of three cycles were simulated making sure that the initial transients disappeared. Further refinement of the time steps did not change the results. Flow was considered pulsatile with a synthetic inlet velocity function reproducing a realistic shape of the cardiac function as demonstrated on Fig. 1. Constant pressure was used as the outlet boundary condition considering the constant nature of the peripheral resistance. More details of the technique are available elsewhere [20].

All aneurysms were then analyzed using 2-D angiograms in two standard planes, the 3-D reconstruction model and the simulated flow pattern. Patient history, lesion location,

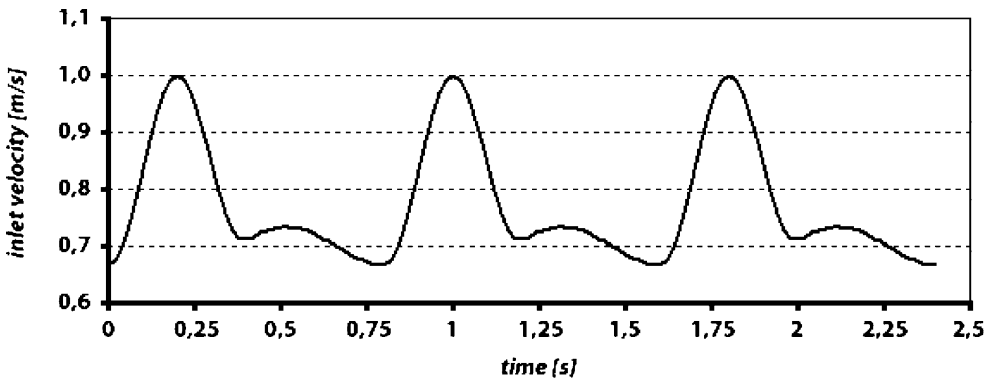

Fig. 1 The simulated inlet velocity function

aneurysm diameters in two planes, aspect ratio, morphological type, aneurysm to parent vessel angle, flow pattern, pressure and shear stress distribution over the aneurysm wall were recorded for each aneurysm. The two largest diameters of each aneurysm were measured in two perpendicular planes selected on 3-D reconstructed images. The aspect ratio was defined as the height of the aneurysm divided by the width of the neck [19].

Aneurysms were categorized as side-wall or bifurcation type on the basis of their morphology. Based on our previous observations using flow studies, we further classified side-wall aneurysms as side-wall type with either a limited focal involvement of one side of the parent artery wall (single-sided) or circumferential involvement of the parent vessel (circumferential; Figs. 2 and 3). Based on similar observations, bifurcation aneurysms were further divided into symmetric and asymmetric bifurcation types based on the symmetry of the aneurysm sac related to the main axis of the parent artery in the plane of the side branches. On 3-D reconstructed images, the main axis of the last straight segment of the parent artery immediately proximal to the aneurysm and the two main axes of the aneurysm (considered as the two largest diameters) were obtained in two perpendicular planes. The angles between the parent artery axis and the two axes of the aneurysm were measured. Aneurysms with axial angles less than 45° in both planes were considered as parallel type and those with an angle of more than 45° in one plane were classified as perpendicular type (Figs. 4 and 5).

Intraaneurysmal flow patterns were characterized as regular vortex flow with inflow at the distal and outflow at the proximal edge of the neck and a single vortex within the sac (Figs. 2e,f and 4e), irregular vortex flow with reversed inflow/outflow zones and/or multiple vortices (Fig. 3e,f) or jet type flow with a straight inflow zone hitting the aneurysm dome that behaved as a flow divider, and outflow either at one or both edges of the neck (Fig. 5e,f). Pressure was recorded on flow simulations and classified as either evenly distributed over the aneurysm surface (Figs. 2, 3 and 4) or having a peak at a small

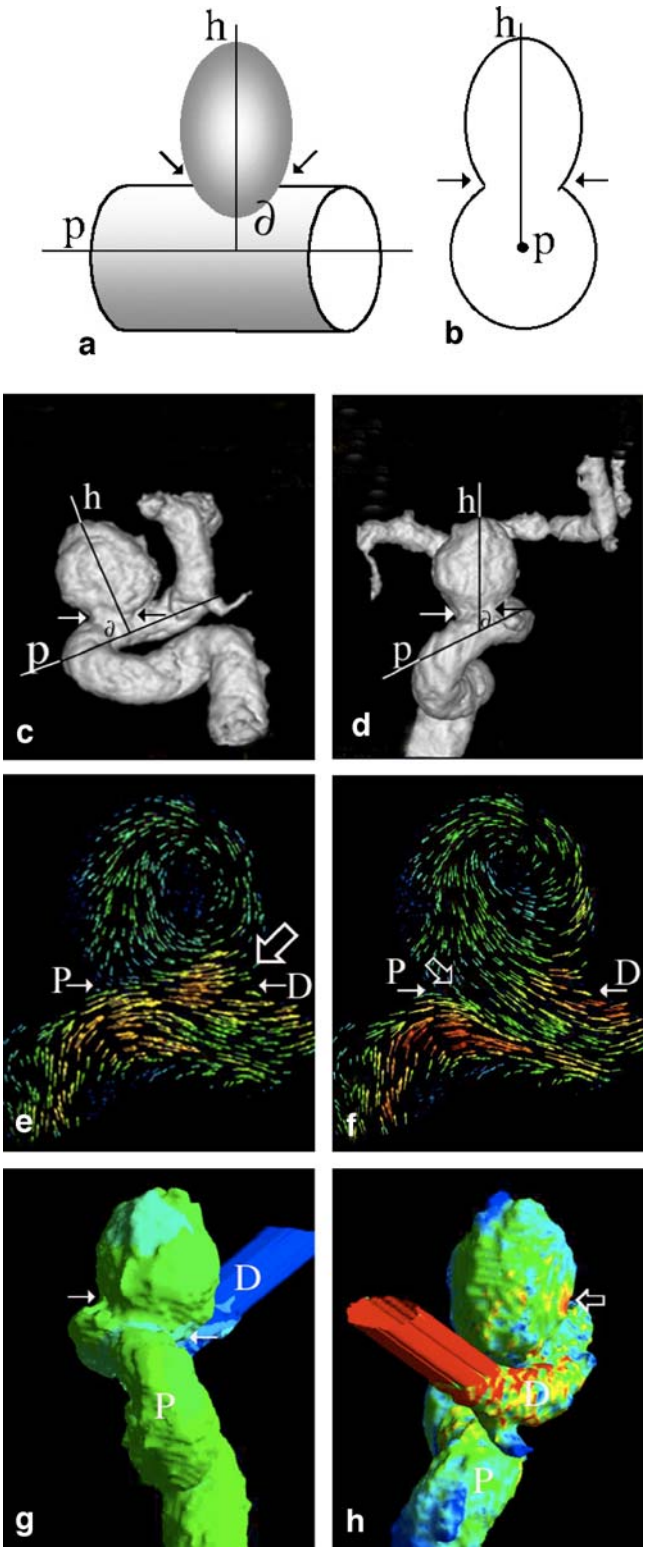

Fig. 2 Geometry and flow characteristics of a single-sided side-wall aneurysm with limited involvement of the parent artery wall. **a**, **b** Schematic depiction of a single-sided side-wall aneurysm in longitudinal (**a**) and cross-sectional (**b**) views (*arrows* edges of the neck). The angle (*∂*) between the main axis of the parent artery (*p*) and the height of the aneurysm (*h*) is 90° (perpendicular type). **c**, **d** 3-D reconstructed images of a paraophthalmic aneurysm in the lateral (**c**) and anteroposterior (**d**) views, with limited single-sided involvement of the parent artery (*arrows* neck). The angle (*∂*) between the height of the aneurysm (*h*) and the axis of the parent artery (*p*) is 70° (lateral) and 65° (anteroposterior) (perpendicular type). **e**, **f** Flow velocity vectors in the longitudinal plane demonstrate the inflow zone (*open arrow*) at the distal edge of the neck (*D*) and the outflow zone at the proximal edge of the neck (*P*). **g** Pressure distribution map of the same aneurysm demonstrates homogeneous distribution over the sac of the aneurysm in the systolic phase (*arrows* neck, *D* distal parent artery, *P* proximal parent artery). **h** Shear stress distribution map of the same aneurysm shows a small area of increased shear stress at the distal edge of the neck (*arrow*) (*D* distal parent artery, *P* proximal parent artery)

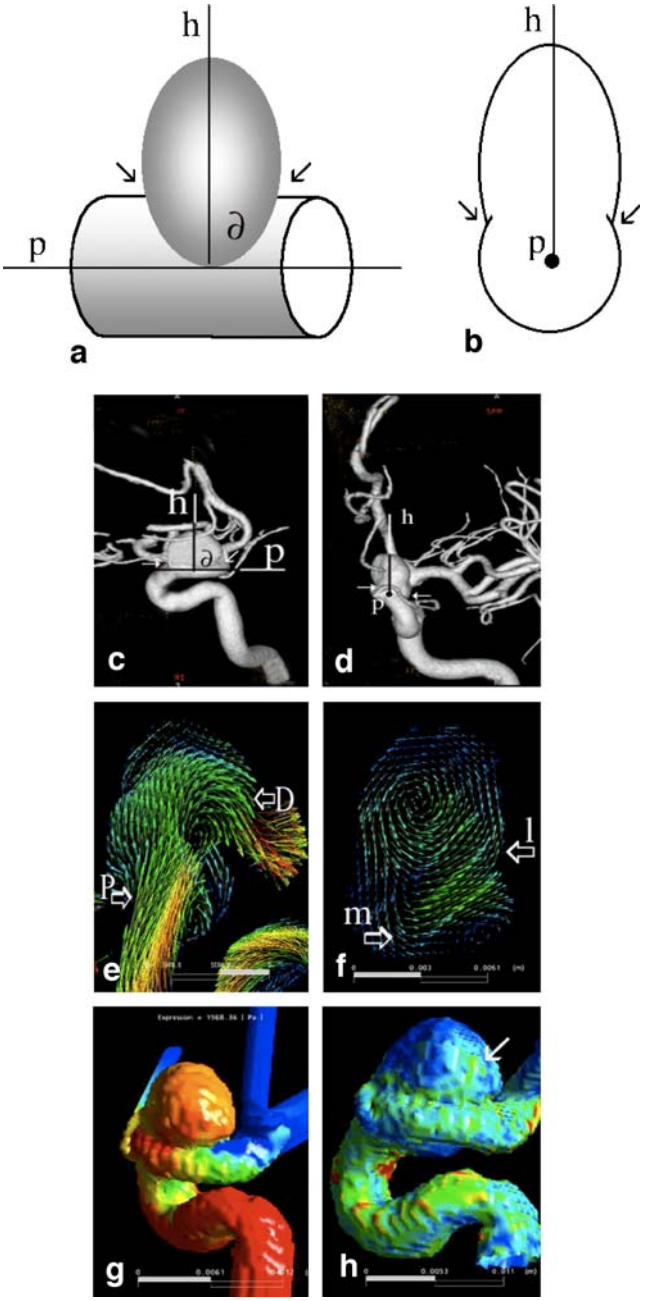

Fig. 3 Geometry and flow characteristics of a circumferential side-wall aneurysm with extended involvement of the parent artery wall. **a**, **b** Schematic depiction of a side-wall aneurysm with extended, circumferential involvement of the parent artery wall in longitudinal (**a**) and cross-sectional (**b**) views (*arrows* edges of the neck. The angle (*∂*) between the main axis of the parent artery (*p*) and the height of the aneurysm (*h*) is 90° (perpendicular type). **c**, **d** 3-D reconstructed images of a paraophthalmic aneurysm in the lateral (**c**) and anteroposterior (**d**) views, with extended circumferential involvement of the parent artery wall (*arrows* neck). The angle (*∂*) between the main axis of the aneurysm (*h*) and the axis the parent artery (*p*) is 70° (lateral) and 65° (anteroposterior) (perpendicular type). **e** Flow velocity vectors in a longitudinal (sagittal) plane demonstrate the inflow zone at the proximal edge (*open arrow*, *P*) and the outflow zone at the distal edge (*open arrow*, *D*) of the neck. **f** Flow velocity vectors in a cross-sectional (frontal) plane demonstrate the inflow zone at the lateral edge (*open arrow*, *l*) and the outflow zone at the medial edge (*open arrow*, *m*) of the neck. Note that in such cases the inflow/outflow zones cannot be interpreted in the proximal/distal frame of reference. The characteristic vortex develops in a plane perpendicular to the main axis of the parent artery. **g** Pressure map of the same aneurysm demonstrates a homogeneous pressure distribution in the systolic phase. **h** Shear stress distribution map demonstrates a homogeneously low shear stress over the wall of the aneurysm except in a small area on the distal part of the sac with slightly increased values (*arrow*)

area of the aneurysm dome (Fig. 5). Shear stress was considered to be evenly distributed or having a peak at the neck or at the dome (Figs. 2, 3 and 5).

Results

Of the 21 aneurysms, 16 were unruptured, and five patients had a history of SAH. The largest dimension of the aneurysms ranged from 6.5 to 20 mm and the aspect ratio from 0.75 to 3.75. Of ten side-wall aneurysms, five were classified as single-sided (Fig. 2) and five as circumferential (Fig. 3). Six of the bifurcation aneurysms were asymmetric and five were symmetric. Considering the aneurysm/parent vessel angle, 14 aneurysms were classified as perpendicular (Figs. 2, 3 and 4) and 7 as parallel (Fig. 5). Regular vortex flow was found in eight aneurysms (Figs. 2 and 4), irregular vortex flow in six (Fig. 3) and jet type flow in seven (Fig. 5). Pressure distribution was even in 11 aneurysms and had a peak in 10 (Fig. 5g), while shear stress was evenly distributed in seven aneurysms, and had a peak at the neck in nine (Fig. 5h) and in the sac in five (Fig. 3h; Table 1). No correlation was found between aneurysm size, neck size, aspect ratio and flow pattern, and pressure or shear stress distribution.

Aneurysm morphology did correlate with location. Nine of ten side-wall aneurysms were located on the supraclinoid internal carotid artery and one on the basilar trunk. No relationship was found between single-sided or circumferential involvement and aneurysm location. Bifurcation aneurysms were located on the basilar artery (three), middle cerebral artery (two) or internal carotid artery (two) bifurcation, on the anterior communicating artery (three) or at a fenestrated vertebrobasilar junction (one). There was a strong correlation between aneurysm/parent vessel angle and flow pattern. All 14 perpendicular aneurysms including ten side-wall and four bifurcation aneurysms had vortex flow (Figs. 2, 3 and 4), while jet flow was seen in seven out of seven parallel aneurysms, and all these were located at bifurcations (Fig. 5; Table 1). Morphological subtype seemed to influence flow pattern: four of five single-sided

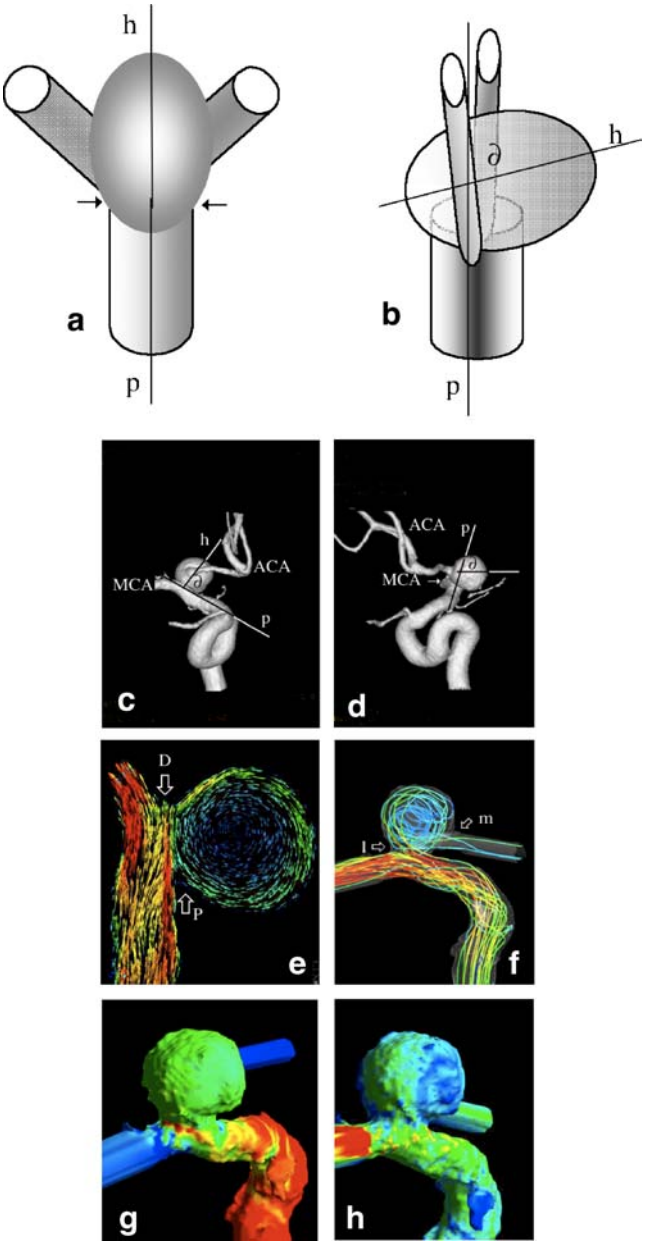

Fig. 4 Geometry and flow characteristics of a bifurcation aneurysm with the main axis of the aneurysm perpendicular to the main axis of the parent artery. **a**, **b** Schematic depiction of a bifurcation aneurysm in two orthogonal views (*arrows* neck). The angle (*∂*) between the main axis of the parent artery (*p*) and the height of the aneurysm (*h*) is 0° in one view (**a**) and 70° in the orthogonal view (**b**) (perpendicular type). **c**, **d** 3-D reconstructed images of a carotid bifurcation aneurysm in the anteroposterior (**c**) and lateral (**d**) views. The angle (*∂*) between the height of the aneurysm (*h*) and the axis of the parent artery (*p*) is 90° in the anteroposterior (**c**) and 60° in the lateral view (**d**) (perpendicular position). **e** Flow velocity vectors in the sagittal plane demonstrate the inflow zone at the proximal edge (*open arrow*, *p*), and a regular vortex within the sac. **f** Slipstreams in the frontal view demonstrate the inflow zone at the lateral (*open arrow*, *l*) and the outflow zone at the medial edge (*open arrow*, *m*) of the neck. A regular vortex is seen within the sac. **g**, **h** Pressure map (**g**) and shear stress map (**h**) of the same aneurysm demonstrate evenly distributed low pressure and shear stress over the wall of the aneurysm

side-wall aneurysms had regular vortex flow (Fig. 2) and four of five circumferential side-wall lesions had irregular vortex flow (Fig. 3). In bifurcation types, a symmetric morphology was associated with jet flow (five of six aneurysms) while three of five aneurysms with an asymmetric morphology had either regular or irregular vortex flow (Table 1).

Pressure distribution did correlate with flow pattern: all 11 aneurysms with even pressure distribution had vortex flow (six regular and five irregular), while seven of ten aneurysms with a pressure peak over the sac had jet flow (Table 1). There was a weak correlation between shear stress distribution and flow pattern: six of seven aneurysms with even shear distribution and seven of nine with a peak at the neck had vortex flow, while four of five with a peak at the dome had jet type of flow (Table 1). All five ruptured aneurysms had a peak of unsteady pressure at the dome and four had parallel geometry. In general, aneurysm to parent vessel angle was found to be the most significant factor determining the flow pattern and subsequently pressure distribution. This feature had more impact on flow than morphological type.

Discussion

With increasing use of less-invasive imaging studies capable of visualizing intracranial vessels, clinicians are faced with a growing difficulty in choosing between the risk of the natural course and that of invasive treatment in an individual patient carrying an incidentally discovered, unruptured intracranial aneurysm, many of which are likely to remain innocent for the rest of the individual's life. In order to set guidelines for treatment indications, the natural history of unruptured aneurysms has been investigated in recent clinical studies which have demonstrated a relationship between the risk of rupture and history, aneurysm size and location. These results suggest that aneurysm location and size are the sole factors responsible for a higher risk of rupture [1, 2]. While the significance of size might be explained by physical phenomena (Laplace's law), the role played by location has not been explained. It seems reasonable to explain the effect of location by an influence of material properties of the surrounding tissues as proposed and demonstrated by Satoh et al. [16, 17] and San Millán Ruiz et al. [15]. Another factor might be intraaneurysmal flow that may also be determined by the anatomical environment in which the aneurysm has grown. In the present study we investigated the relationships between different geometrical features (other than the size of the aneurysm sac and neck) and flow patterns, anticipating that these may affect both treatment results and natural history.

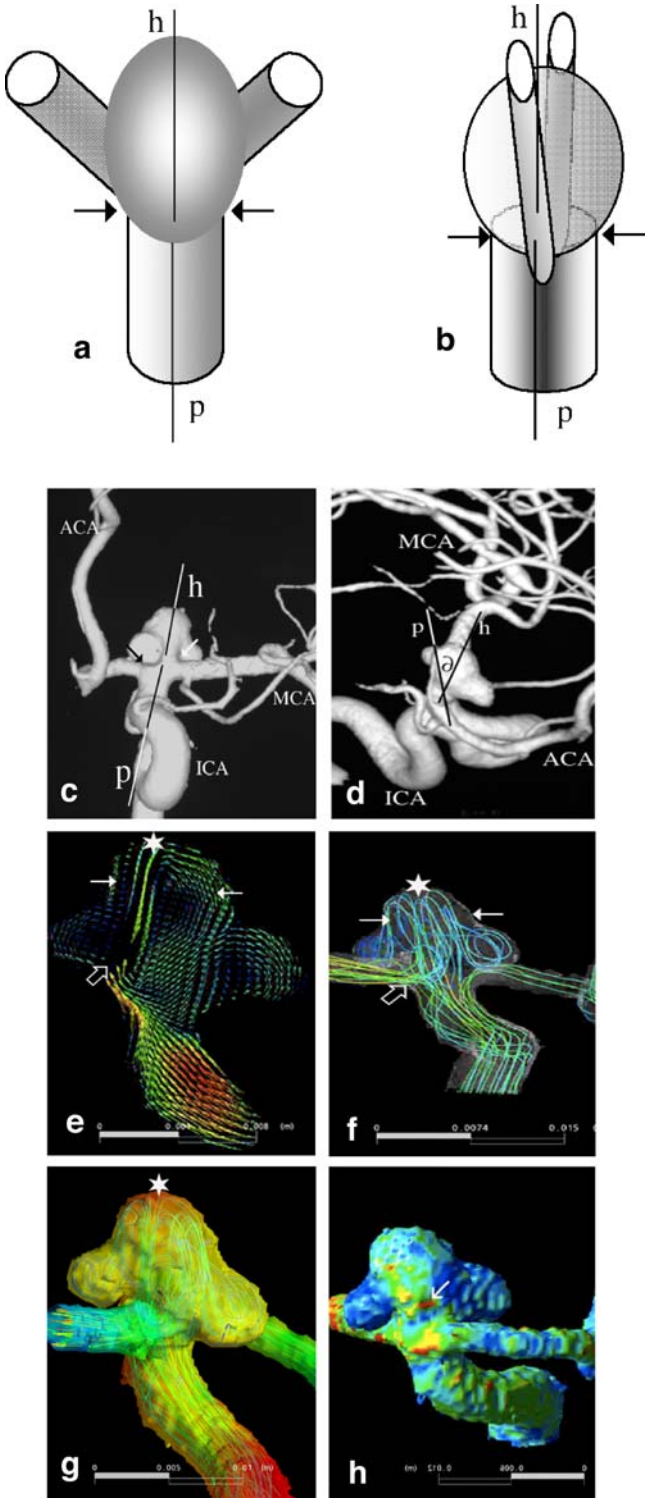

Fig. 5 Geometry and flow characteristics of a bifurcation aneurysm with the main axis of the aneurysm parallel to the main axis of the parent artery. **a**, **b** Schematic depiction of a bifurcation aneurysm with the main axis of the aneurysm parallel to the main axis of the parent artery in two orthogonal views (*arrows* neck). The angle (∂) between the main axis of the parent artery (*p*) and the height of the aneurysm (*h*) is 0° (parallel type). **c**, **d** 3-D reconstructed images of a carotid bifurcation aneurysm in the anteroposterior (**c**) and lateral (**d**) views (*arrows* neck). The angle (∂) between the main axis of the aneurysm (*h*) and the axis of the parent artery (*p*) is 0° (anteroposterior) and 35° (lateral) (parallel type). **e**, **f** Flow velocity vectors (**e**) and slipstreams (**f**) in the frontal plane demonstrate the inflow zone at the medial edge (**e** *open arrow*), a flow divider at the dome (*asterisk*), double vortices (*arrows*) within the sac and the outflow at the medial edge of the neck (**f** *open arrow*). **g** Pressure map of the same aneurysm demonstrates pressure corresponding to the flow divider point (*asterisk*). **h** Shear stress distribution map demonstrates a small area of increased shear stress at the neck (*arrow*)

In early in-vitro studies using transparent tube and in-vivo surgical animal aneurysm models, distinct flow patterns characteristic of different morphological types of aneurysm have been established. Based on these findings, the expected flow pattern is frequently used as a guide for recommending treatment and/or selection of the treatment method. Typical flow patterns include vortex flow for side-wall aneurysms and jet flow in bifurcation/terminal aneurysms. Vortex flow is characterized by a distinct inflow zone at the distal edge, an outflow zone at the proximal edge of the aneurysm neck and vortex flow within the center of the aneurysm [3]. This type of intraaneurysmal flow is primarily driven by shear at the entrance of the aneurysm sac and is similar to the shear-driven endosaccular flow phenomenon described by fluid dynamics. Inflow and outflow zones are located in different but parallel planes distal and proximal to the aneurysm neck. Jet flow is defined by an inflow zone directly hitting the aneurysm dome and exiting either at both or just one side of the neck [4]. The impact of the entering zone on coil compaction/aneurysm recanalization has been highlighted [3]. Flow studies in experimental aneurysm models have shown the impact of aneurysm geometry as described by the aspect ratio (defined as the ratio of the height of aneurysm and width of the neck) [19]. We have confirmed the effects of the aspect ratio and of the width of the neck in previous work on idealized computer models of side-wall aneurysms [20].

With the advent of 3-D aneurysm visualization by catheter or CT angiography, CFD simulation of aneurysm flow has become feasible and is now widely used in models based on clinical data [10–13, 20]. This technique has been applied to analyze the effect of hemodynamic factors on natural history. In a large study consisting of 62 "real" aneurysms an association was found between an unstable flow pattern, a small flow impingement area on the dome and a narrow inflow jet and the incidence of aneurysm rupture [21]. In another study, a positive correlation was found between aspect ratio and the incidence of rupture in side-wall aneurysms, but not in bifurcation aneurysms [18].

In the present study, aneurysms were selected in a retrospective manner focusing on morphological features, making sure that formerly established morphological sub-

Table 1 Clinical, geometrical and flow characteristics of aneurysms

Location	History of SAH		Size (mm)		Aspect ratio	Aneurysm type		Morphological type				Flow pattern			Pressure distribution		Shear stress distribution		
	Yes	No	Aneurysm	Neck		Perpendicular[a]	Parallel[b]	Side-wall		Bifurcation		Regular vortex	Irregular vortex	Jet	Even	Peak at dome	Even	Peak at neck	Peak at dome
								Single-sided	Circumferential	Symmetric	Asymmetric								
Posterior communicating artery		1	13	4	3.75	1		1					1		1			1	
Ophthalmic artery		1	9	5	1.40	1			1				1		1			1	
Ophthalmic artery		1	9	10	0.75	1			1				1			1	1		
Ophthalmic artery		1	10	6	1.00	1			1				1		1		1		
Internal carotid artery bifurcation		1	8	3	2.67	1				1		1			1			1	
Internal carotid artery		1	18	11	1.82	1			1				1		1		1		
Basilar artery	1		15	8	2.13	1			1			1				1		1	
Anterior communicating artery		1	18	6	2.50	1					1	1			1		1		
Vertebrobasilar junction		1	9	5	2.60	1					1	1			1		1		
Posterior communicating artery		1	10	5	2.40	1		1				1			1			1	
Ophthalmic artery		1	8	5	1.60	1		1				1			1		1		
Basilar artery		1	10	7	1.29	1					1		1		1				1
Ophthalmic artery		1	10	6	1.67	1		1				1			1			1	
Posterior communicating artery		1	11	3	3.33	1		1				1				1		1	
Anterior communicating artery	1		6	3.7	1.27		1				1			1		1			1

Table 1 (continued)

Location	History of SAH		Size (mm)		Aspect ratio	Aneurysm type		Morphological type				Flow pattern			Pressure distribution		Shear stress distribution		
	Yes	No	Aneurysm	Neck		Perpendicular[a]	Parallel[b]	Side-wall		Bifurcation		Regular vortex	Irregular vortex	Jet	Even	Peak at dome	Even	Peak at neck	Peak at dome
								Single-sided	Circumferential	Symmetric	Asymmetric								
Anterior communicating artery		1	7	5	1.20		1				1			1		1			1
Middle cerebral artery		1	8	5	1.80		1			1				1		1			1
Middle cerebral artery		1	10	5	2.40		1			1				1		1		1	
Basilar artery	1		8	5	1.20		1			1				1		1	1		
Internal carotid artery bifurcation	1		9	4	1.50		1			1				1		1		1	
Basilar artery	1		9	6.5	1.23		1			1				1		1			1
Mean			10	6	2														
Total	5	16				14	7	5	5	6	5	8	6	7	11	10	7	9	5

[a] Perpendicular type: angle >45° between the axis of the parent artery and axis of the aneurysm in one plane.
[b] Parallel type: angle <45° between the axis of the parent artery and axis of the aneurysm in both planes.

types with characteristic flow patterns, such as side-wall and bifurcation aneurysms, were equally represented in the study population. Earlier we had found that the involvement of the parent artery wall in the aneurysm neck greatly affects intraaneurysmal flow and so side-wall aneurysms were further divided into those with focal involvement of the arterial wall (single-sided) and those with larger circumferential involvement (Figs. 2 and 3).

In the simulation studies, parent vessels and aneurysms were considered as rigid tubes. Although theoretically vessel wall motion may have a significant impact on flow, this practice is justified by both our previous research incorporating vessel wall material properties into coupled simulations (unpublished data) and studies using high frame-rate angiographic images to detect geometrical changes of the aneurysm wall over the course of the cardiac cycle [22]. Both studies demonstrated little effect of wall elasticity on flow. A synthetic inlet velocity function was used to simulate pulsatile flow. This is acceptable, as previous studies have proved that the characterization of intraaneurysmal flow is not altered by the mean input flow or flow divisions [23]. Constant pressure was used as the outlet boundary condition considering the constant nature of the peripheral resistance. In theory, the resistance of the entire arterial system between the studied segment and the capillary level should be modeled. In our earlier work we found that while using incompressible fluids and rigid walls for the simulation, the addition of a mimicked capillary resistance in the form of a porous material only adds an additive constant to the pressure level, but does not change the resulting flow velocity field. Therefore—for the sake of faster simulation—we omitted the porous material mimicking capillary resistance. This would have more significance if flexible tubes were simulated.

Traditionally, flow in side-wall aneurysms is considered vortex type and in bifurcation aneurysms jet type. Most studies describing these flow patterns have been based on either glass or silicon aneurysm models, surgically created experimental aneurysms or 2-D angiograms. Generally used models of side-wall aneurysms typically have regular geometry and small, well-circumscribed involvement of a small surface of the parent artery [24]. Similarly, models of bifurcation aneurysms are usually positioned within the straight continuation of the main axis of the parent artery and most are symmetrically oriented in between the two side branches. In contrast to the above, in our early experiments we found that the locations of the inflow and outflow zones are not necessarily arranged distally and proximally as previously thought in side-wall aneurysms, and jet flow is not always a characteristic feature of bifurcation aneurysms either. Based on these observations, we hypothesized that significant circumferential involvement of the parent artery wall within the orifice of the aneurysm may change the plane of the vortex and the location of the inflow and outflow tracks. Similarly, we assumed that significant divergence of the main axis of the aneurysm from that of the parent artery might influence the jet flow pattern.

To test these assumptions, with further morphological analysis of side-wall aneurysms based on 3-D images, we classified aneurysms with limited involvement of the parent artery wall less than one-quarter of its circumference as single-sided side-wall aneurysms (Fig. 2) and those with more than one-quarter of the parent artery wall missing (resulting in an aneurysm neck circumferentially involving the artery) as circumferential side-wall aneurysms (Fig. 3). Four of five single-sided aneurysms had regular vortex flow (Fig. 2e,f) and four of five circumferential aneurysms had irregular vortex flow with the inflow/outflow zones being reversed or complex (Fig. 3e,f).

The impact of neck width on flow velocities has been previously described either in relation to the aneurysm height (aspect ratio) [19] or as a factor affecting the magnitude of rotational motion within the vortex [20]. However, these studies considered the width of the neck only, that is the diameter of the neck alongside the main axis of the parent artery. The current observations suggest that the size of the neck in a plane perpendicular to the parent vessel axis also plays a role by changing the flow pattern of the aneurysm. With circumferential involvement, the aneurysm sac is not necessarily positioned symmetrically on top of the parent artery. If the sac is arranged in an asymmetric fashion, the shear-driven vortex flow may develop in a plane perpendicular to the parent artery axis rather than in the parallel plane as generally thought. This may explain the reversal of the locations of the inflow/outflow zones, since proximal or distal positions cannot be interpreted in a plane perpendicular to the main stream of flow within the parent vessel (Fig. 3).

Similar to the above, bifurcation aneurysms were classified based on the angle between the height of the aneurysm and the main axis of the parent artery. We measured this angle, and considered those aneurysms with an angle >45° as perpendicular types (Fig. 4) and those with an angle <45° as parallel types (Fig. 5). As expected, all side-wall aneurysms were perpendicular, but not all bifurcation aneurysms were parallel to the parent artery. The axis of 4 of 11 bifurcation aneurysms diverged significantly from the axis of the parent artery (Fig. 4). All perpendicular aneurysms had vortex flow (either regular or irregular), including four bifurcation aneurysms. On the other hand, all seven parallel aneurysms had jet flow (Fig. 5), and were bifurcation aneurysms. Previously vortex flow was thought to be a typical feature of side-wall aneurysms and jet flow has been generally associated with bifurcation aneurysms [3, 25]. These results, however, suggest that the shear-driven versus jet type nature

of the flow pattern is primarily determined by the aneurysm/parent vessel angle rather than by the side-wall or bifurcation configuration of the lesion.

As in previous studies [21], we found a strong correlation between flow type and unsteady pressure distribution: all seven aneurysms with jet flow had an uneven distribution with a peak at the dome, while 11 of 14 with vortex flow had an even distribution of pressure along the wall of the aneurysm sac. In this latter group, flow irregularities did not seem to influence pressure distribution. The significance of this finding is debatable. In an earlier study of idealized 2-D aneurysm models, pressure peaks at the apex of aneurysms exceeded by two to three times those measured within the parent artery [24]. In other studies, pressure elevation in the aneurysm dome was only 1–2% of the peak intravascular pressure [26]. In our experience, the magnitude of pressure inhomogeneity was very low, with intraaneurysmal peaks not exceeding the maximum pressure within the parent artery. However, even at low magnitudes, coupled spatial and temporal inhomogeneity may play a role in aneurysm wall fatigue and eventual rupture. Clinically, four of five ruptured aneurysms in the study group had a parallel axis, jet flow and peak pressure at the dome.

The distribution of shear stress is generally considered as a potentially significant factor in aneurysm growth and rupture. There is, however, significant confusion in the literature concerning the interpretation of wall shear inhomogeneity. Low shear stress has been associated with aneurysm growth [27] and elevated shear stress with aneurysm rupture [28]. Other researchers found a markedly low shear stress at the apex of ruptured aneurysms and have proposed that low shear may induce degenerative processes within the aneurysm wall leading to rupture, while high shear stress at the neck may result in aneurysm growth [29]. In our study, the spatial distribution of shear stress demonstrated a weak correlation with flow pattern: 13 of 14 aneurysms with vortex flow either had an even distribution or a peak shear stress at the neck while 4 out of 7 with jet flow had a peak shear stress at the dome. We could not establish any correlation between clinical course and shear stress distribution in this study.

Conclusion

Aneurysmal geometry has a significant impact on intraaneurysmal flow conditions. Circumferential involvement of the parent artery wall modulates the characteristic flow pattern of side-wall aneurysms and may result in reversed inflow/outflow zones. This feature should be considered in treatment planning. In this study, the aneurysm/parent vessel angle was the primary factor determining the basic flow pattern of the aneurysm. Aneurysms perpendicular to the parent artery had shear-driven, vortex flow and those parallel to the parent artery had jet flow, regardless of whether they were located on the side-wall or at a bifurcation of the parent artery. Jet flow seems to induce an uneven pressure distribution over the aneurysm wall, and might be more frequently associated with aneurysm rupture. This may have implication in treatment planning. The degree of arterial wall involvement and the degree of deviation of the aneurysm axis from the parent artery axis associated with such flow disturbances cannot be established from the current study and needs further investigations. As the number of aneurysms investigated in our study was too small to draw statistically valid conclusions, further studies are needed to validate these observations and confirm their clinical relevance.

Acknowledgements This study was supported in part by a grant from the Hungarian National Science and Research Foundation (no. T 047150 OPR) and by research support from GE Amersham Healthcare Hungary.

Conflict of interest statement We declare that we have no conflict of interest.

References

1. ISUIA Investigators (1998) Unruptured intracranial aneurysms – risk of rupture and risks of surgical intervention. International Study of Unruptured Intracranial Aneurysms Investigators. N Engl J Med 339(24):1725–1733
2. ISUIA Investigators (2003) Unruptured intracranial aneurysms: natural history, clinical outcome, and risks of surgical and endovascular treatment. Lancet 362:103–110
3. Graves VB et al (1992) Flow dynamics of lateral carotid artery aneurysms and their effects on coils and balloons: an experimental study in dogs. AJNR Am J Neuroradiol 13(1):189–196
4. Kerber CW et al (1996) Flow dynamics in a fatal aneurysm of the basilar artery. AJNR Am J Neuroradiol 17(8):1417–1421
5. Strother CM (1995) In vitro study of haemodynamics in a giant saccular aneurysm model: influence of flow dynamics in the parent vessel and effects of coil embolisation. Neuroradiology 37 (2):159–161
6. Tateshima S et al (2001) Intraaneurysmal flow dynamics study featuring an acrylic aneurysm model manufactured using a computerized tomography angiogram as a mold. J Neurosurg 95 (6):1020–1027
7. Valencia A (2004) Flow dynamics in models of intracranial terminal aneurysms. Mech Chem Biosyst 1(3):221–231
8. Valencia AA et al (2006) Blood flow dynamics in saccular aneurysm models of the basilar artery. J Biomech Eng 128 (4):516–526
9. Foutrakis GN, Yonas H, Sclabassi RJ (1997) Finite element methods in the simulation and analysis of intracranial blood flow. Neurol Res 19(2):174–186
10. Chong BW et al (1994) Blood flow dynamics in the vertebrobasilar system: correlation of a transparent elastic model and MR angiography. AJNR Am J Neuroradiol 15(4):733–745

11. Jou LD et al (2003) Computational approach to quantifying hemodynamic forces in giant cerebral aneurysms. AJNR Am J Neuroradiol 24(9):1804–1810
12. Castro MA, Putman CM, Cebral JR (2006) Computational fluid dynamics modeling of intracranial aneurysms: effects of parent artery segmentation on intra-aneurysmal hemodynamics. AJNR Am J Neuroradiol 27(8):1703–1709
13. Cebral JR, Lohner R (2005) Efficient simulation of blood flow past complex endovascular devices using an adaptive embedding technique. IEEE Trans Med Imaging 24(4):468–476
14. Burleson AC, Strother CM, Turitto VT (1995) Computer modeling of intracranial saccular and lateral aneurysms for the study of their hemodynamics. Neurosurgery 37(4):774–782, discussion 782–784
15. San Millán Ruiz D et al (2006) The perianeurysmal environment: influence on saccular aneurysm shape and rupture. AJNR Am J Neuroradiol 27:504–512
16. Satoh T et al (2005) Influence of perianeurysmal environment on the deformation and bleb formation of the unruptured cerebral aneurysm: assessment with fusion imaging of 3D MR cisternography and 3D MR angiography. AJNR Am J Neuroradiol 26(8):2010–2018
17. Satoh T et al (2005) Visualization of aneurysmal contours and perianeurysmal environment with conventional and transparent 3D MR cisternography. AJNR Am J Neuroradiol 26(2):313–318
18. Hassan T et al (2005) A proposed parent vessel geometry-based categorization of saccular intracranial aneurysms: computational flow dynamics analysis of the risk factors for lesion rupture. J Neurosurg 103(4):662–680
19. Ujiie H et al (1999) Effects of size and shape (aspect ratio) on the hemodynamics of saccular aneurysms: a possible index for surgical treatment of intracranial aneurysms. Neurosurgery 45 (1):119–129, discussion 129–130
20. Paal G et al (2007) Flow in simplified and real models of intracranial aneurysms. Int J Heat Fluid Flow 28:653–664
21. Cebral JR et al (2005) Characterization of cerebral aneurysms for assessing risk of rupture by using patient-specific computational hemodynamics models. AJNR Am J Neuroradiol 26 (10):2550–2559
22. Cebral J (2007) Personalized computational modeling of stented cerebral aneurysms. Paper presented at the 4th International Intracranial Stent Meeting, Kyoto, Japan, 18–20 April 2007
23. Cebral JR et al (2005) Efficient pipeline for image-based patient-specific analysis of cerebral aneurysm hemodynamics: technique and sensitivity. IEEE Trans Med Imaging 24(4): 457–467
24. Foutrakis GN, Yonas H, Sclabassi RJ (1999) Saccular aneurysm formation in curved and bifurcating arteries. AJNR Am J Neuroradiol 20(7):1309–1317
25. Kerber CW, Heilman CB (1983) Flow in experimental berry aneurysms: method and model. AJNR Am J Neuroradiol 4 (3):374–377
26. Shojima M et al (2005) Role of the bloodstream impacting force and the local pressure elevation in the rupture of cerebral aneurysms. Stroke 36(9):1933–1938
27. Jou LD et al (2005) Correlation between lumenal geometry changes and hemodynamics in fusiform intracranial aneurysms. AJNR Am J Neuroradiol 26(9):2357–2363
28. Hassan T et al (2004) Computational replicas: anatomic reconstructions of cerebral vessels as volume numerical grids at three-dimensional angiography. AJNR Am J Neuroradiol 25 (8):1356–1365
29. Shojima M et al (2004) Magnitude and role of wall shear stress on cerebral aneurysm: computational fluid dynamic study of 20 middle cerebral artery aneurysms. Stroke 35(11):2500–2505